Single- and Two-State Reactivity in the Gas-Phase C–H Bond Activation of Norbornane by 'Bare' FeO^+

by **Nathan Harris** and **Sason Shaik***

Department of Organic Chemistry and the Lise-Meitner-Minerva Center for Computational Quantum Chemistry, The Hebrew University of Jerusalem, 91904 Jerusalem, Israel

and **Detlef Schröder** and **Helmut Schwarz***

Institut für Organische Chemie der Technischen Universität Berlin, Straße des 17. Juni 135, D-10623 Berlin

Dedicated to Prof. *N. M. M. Nibbering*, Amsterdam, on the occasion of his 60th birthday

The potential-energy surface for C–H bond activation of norbornane by 'bare' FeO^+ is examined at the B3LYP/6-31G** level of theory. The free reactants combine to form norbornane/FeO^+ ion-dipole clusters in which the FeO^+ unit can bind at either the *exo* or *endo* face of norbornane. The transition structures for insertion of FeO^+ into the *exo* and *endo* C–H bonds are located at least 9 kcal · mol^{-1} below the entrance channel, thus accounting for the observed unit efficiency of the C–H bond activation reported in previous gas-phase ion-cyclotron resonance experiments (*Helv. Chim. Acta* **1995**, *78*, 1013). Interesting features of the reaction profiles are crossovers of the high-spin sextet (S = 5/2) and low-spin quartet (S = 3/2) states *en route* to the transition structures (TS); this type of behavior has been termed two-state reactivity (*Helv. Chim. Acta* **1995**, *78*, 1393). The branchings between the *endo* and *exo* pathways are simulated by *Rice-Ramsperger-Kassel-Marcus* (*RRKM*) theory with the calculated harmonic frequencies. Additionally, hydrogen/deuterium kinetic isotope effects are computed using *RRKM* theory and compared with the experimental data. The simulated KIEs differ for high-spin and low-spin TSs, suggesting that isotope effects can be used as sensitive probes for diagnosing spin-crossover mechanisms.

1. Introduction. – Gas-phase C–H bond activation of hydrocarbons by transition-metal cations has been studied by mass-spectrometric experiments [1] and by theoretical modeling [2]. Density functional theory (DFT) [3] is particularly suited for theoretical studies of potential-energy profiles of transition-metal compounds as it allows to examine medium-sized systems with reasonable accuracy at moderate costs [2]. The gas-phase studies give an understanding of how and why transition-metal catalysts are able to activate even very inert hydrocarbons.

Several studies of the gas-phase reactivity of 'bare' FeO^+ cation have been made with hydrogen [4], methane [5], benzene [6], and several other organic substrates [7]. Hallmarks are the formal hydroxylations of C–H bonds observed with FeO^+, because of its relevance to biocatalysts such as cytochrome P-450 [8–11] and methane monoxygenase [12], which bear high-valent iron-oxo units as key parts of the active sites.

Here, we report results of DFT modeling of the C–H bond activation of norbornane by FeO^+ in the gas phase (*Scheme 1*). Norbornane is a particularly interesting substrate, because it is a structural analog of camphor, which is the substrate for $P\text{-}450_{cam}$ from the soil bacterium *Pseudomonas putida* [8a][9b][13]. Experimental

studies of the FeO^+/norbornane system [14] revealed that the *endo* C–H bonds are activated preferentially and that the reaction is associated with significant intramolecular deuterium kinetic isotope effects (KIEs). From the gas-phase measurements, the *exo*/*endo* branching ratio and KIEs were derived indirectly by product analysis with deuterium-labeled norbornanes as $k_{endo}/k_{exo} = 10.3$, $KIE_{endo} = 2.4$, and $KIE_{exo} = 7.7$ [14a]. The initial products of C–H bond activation are short-lived, and the previous mechanistic conclusions were based on analysis of secondary products. The preferred *endo* C–H bond activation in the gas phase contrasts with results for P-450 and model oxoferryl complexes, which prefer *exo* C–H bond activation [8a][8d][9a][9c][13], but is in accord with the results of permanganate oxidation [9c]. An interesting feature in *Scheme 1* concerns the KIEs, which strikingly differ for the activation of the *exo* and *endo* C–H bonds. These unusual, yet unexplained features form the main stimulus and focus of the present paper.

Scheme 1

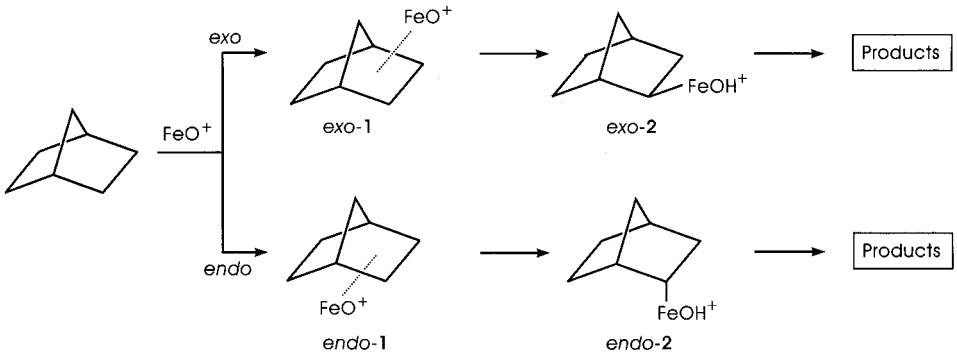

k_{endo}/k_{exo} = 10.3, KIE_{exo} = 7.7, KIE_{endo} = 2.4 [13a]

An important aspect revealed by previous theoretical studies is that the H_2/FeO^+ and CH_4/FeO^+ reactions [4][5] follow a two-state reactivity (TSR) mechanism [4c][15], which has been proposed to be also of prime importance in P-450 hydroxylations, in competition with a single-state reactivity (SSR) [16]. The key issue of TSR is a spin crossover from a high-spin state (here: sextet) in the reactants to a low-spin state (here: quartet) in the products along the reaction coordinate, while, in the different variants of SSR, the rate-determining steps involve a single spin surface. Occurrence of spin crossover along the reaction coordinate may lead to a pronounced SSR/TSR competition, to be examined in the present study.

Besides the questions about spin states and *endo*/*exo* face selectivities, there is another mechanistic question about whether C–H bond activations by FeO^+ (and other transition-metal oxides) occur *via* a concerted four-center mechanism or by a non-concerted three-center mechanism (see *a vs. b* in *Scheme 2*) [4][5]. The radical-type three-center mechanism is assumed to be important in P-450 hydroxylation by the rebound mechanism [8]. In the four-center mechanism, the Fe–C and O–H bonds are formed simultaneously as the Fe–O unit inserts into the C–H bond. The three-center

mechanism is a simple atom transfer with a nearly linear transition structure, whereas the four-centered mechanism can experience an entropic bottleneck [4]. A third possible mechanism is the concerted oxene insertion (*c* in *Scheme 2*) [4g][17], which would directly lead to the hydroxylated product. We do not explore this mechanism here, although its relevance in P-450 hydroxylations has been proposed [8][16b][17].

Scheme 2

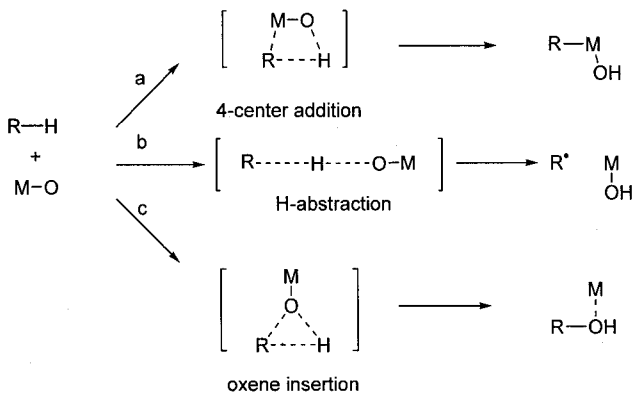

2. Results and Discussion. – Unlike the previous experimental studies, our theoretical treatment[1]) is entirely confined to the very first mechanistic step, *i.e.*, the C–H bond activations in the reactant complexes norbornane/FeO^+ **1** to yield the corresponding insertion intermediates **2** according to *Scheme 1*. The subsequent fragmentations of the insertion species are not addressed any further, and we assume C–H bond activation to be rate-limiting. The validity of the latter assumption is supported by the observation that the reactions of *exo*- and *endo*-norborneol with Fe^+ lead to product distributions similar to those obtained from the norbornane/FeO^+ couple [14].

Reactants. Free FeO^+ has a high-spin $^6\Sigma^+$ ground state [22][23], which has a $1\sigma^2 2\sigma^2 3\sigma^1 1\pi^4 2\pi^2 1\delta^2$ configuration in the valence space [4c]. Thus, the unpaired spins reside in the slightly anti-bonding 3σ, the anti-bonding 2π, and the non-bonding 1δ orbitals. Except for the 1δ occupation, the electronic configuration of FeO^+ ($^6\Sigma^+$) resembles the $^3\Sigma_g^-$ ground state of O_2. Similarly, the low-lying excited quartet states of FeO^+ resemble the $^1\Delta_g$ state of O_2, in which the two π^* electrons are spin-paired [15]. In analogy to the reactivity of O_2 in the triplet and singlet states, we expect the quartet

---

[1]) Calculations were carried out on *DEC Alpha* workstations and on a *Cray J932* in parallel mode with the Gaussian 94 program [18]. Preliminary geometry optimizations were made at the B3LYP/3-21G* level of theory. This level uses the *Becke-3-Lee-Yang-Parr* hybrid density-functional theory [19] together with 3-21G* split-valence basis sets [3c][20]. Following calculations of geometries and frequencies at the B3LYP/3-21G* level, geometries and energies were recalculated with the *Pople* 6-31G** basis sets [3c][20] for C, H, and O, and *Ahlrichs'* valence triple-zeta (VTZ) basis set for iron [21]. For the sake of brevity, this approach is denoted as B3LYP/6-31G**. Once the stationary points (minima and transition structures) were located with the larger basis set, harmonic vibrational frequencies were computed for the key structures. These frequencies were used in evaluating the *endo*/*exo* branching ratios and H/D kinetic isotope effects for [*exo*-2-D_1] and [*endo*-2-D_1]norbornane as substrates.

state of FeO^+ to undergo concerted four-center insertions into C–H bonds with low energy barriers, whereas the sextet state is predicted to react by radical-type three-center mechanisms (see *Scheme 2*). Our computed quartet state of FeO^+ is not a pure eigenfunction of the spin operator. It corresponds to a mixture of quartet states contaminated by higher spin states. Thus, a high/low spin gap of only 7.1 kcal mol^{-1} in the free reactants is computed with our DFT approach, while previous CASPT2D calculations on the lowest quartet state ($^4\Phi$) gave a high/low spin energy difference of *ca.* 0.5 eV (12 kcal · mol^{-1}) [4c][22]. Assuming this value is accurate, our mixed low-spin state is too stable, partly as a consequence of spin contamination, and partly as a general deficiency of DFT in preferring low-spin situations. When the quartet/sextet gap is recomputed according to restricted open-shell theory (RO-DFT), which eliminates spin contamination, the high/low spin gap increases to 18 kcal · mol^{-1}. Accordingly, the DFT calculations[2]) overestimate the stability of the low-spin complexes by a few kcal · mol^{-1}.

Reactant Clusters. The norbornane/FeO^+ reactant cluster was never detected in gas-phase experiments, nor were the primary products of C–H bond activations; the only available clues about the mechanism came from an analysis of the secondary products, which must rely on several assumptions [14]. The experimental data indicate that C–H bond activation takes place regioselectively at the *exo* and *endo* C–H bonds; the other C–H bonds at the bridgehead tertiary C-atoms C(1) to C(6) as well as at the CH_2 bridge, C(7), are not activated [13][14]. In our calculations, the high-spin (HS) and low-spin (LS) reactant clusters *exo*-**1** (HS), *exo*-**1** (LS), *endo*-**1** (HS), and *endo*-**1** (LS) are characterized by agostic bonding of the FeO^+ ion with the C–H bonds of norbornane (*Fig. 1*). In the *exo* clusters, agostic bonding involves one of the *exo* C–H bonds and the *syn* C–H bond of the bridging CH_2 group. In the *endo* cluster, the Fe-atom makes agostic contacts with the four *endo* C–H bonds. The agostic bonds are characterized by close Fe–H and Fe–C non-bonded contacts of *ca.* 2.0 Å and 2.4 Å, elongated C–H bonds of *ca.* 1.12 Å, and narrowing of the corresponding H–C–H angles (*Fig. 1*). Despite the agostic interactions, electrostatics prevail, and the ground states of the reactant clusters arise from the sextet surface of the separated reactants. Analysis of *Mulliken* populations indicates that not only is norbornane polarized considerably by contact with FeO^+, but the charges also show that 0.22–0.24 e is transferred to FeO^+ in forming the reactant *endo* and *exo* complexes. Unlike FeO^+, which is coordinatively unsaturated, oxidants such as MnO_4^-, CrO_2Cl_2, and ferryl porphyrins (*e.g.*, P-450) that are fully coordinated around the metal are less capable of forming agostic contacts [8][16][24][25].

As seen in *Fig. 2*, the computed B3LYP/6-31G** binding energy is 37.5 kcal · mol^{-1} for the most stable *endo*-**1** (HS) cluster. This figure is considered to be slightly overestimated because of the insufficient iron basis set, which results in a basis-set superposition error (BSSE) [26]. A counterpoising calculation [26] gives an estimate of 7.7 kcal · mol^{-1} for the overbinding error. Note that the smaller 3-21G* basis gives much larger BSSEs; *e.g.*, the computed B3LYP/3-21G* binding energy of *endo*-**1** (HS) is as large as 70 kcal · mol^{-1}. Considering the well-depths and the size of the system, the clusters are considered to be long-lived in the sense that the binding energy is

---

[2]) A crucial, so far unanswered issue in DFT concerns how the absolute and relative errors between different spin surfaces affect the relative heights of the computed transition structures.

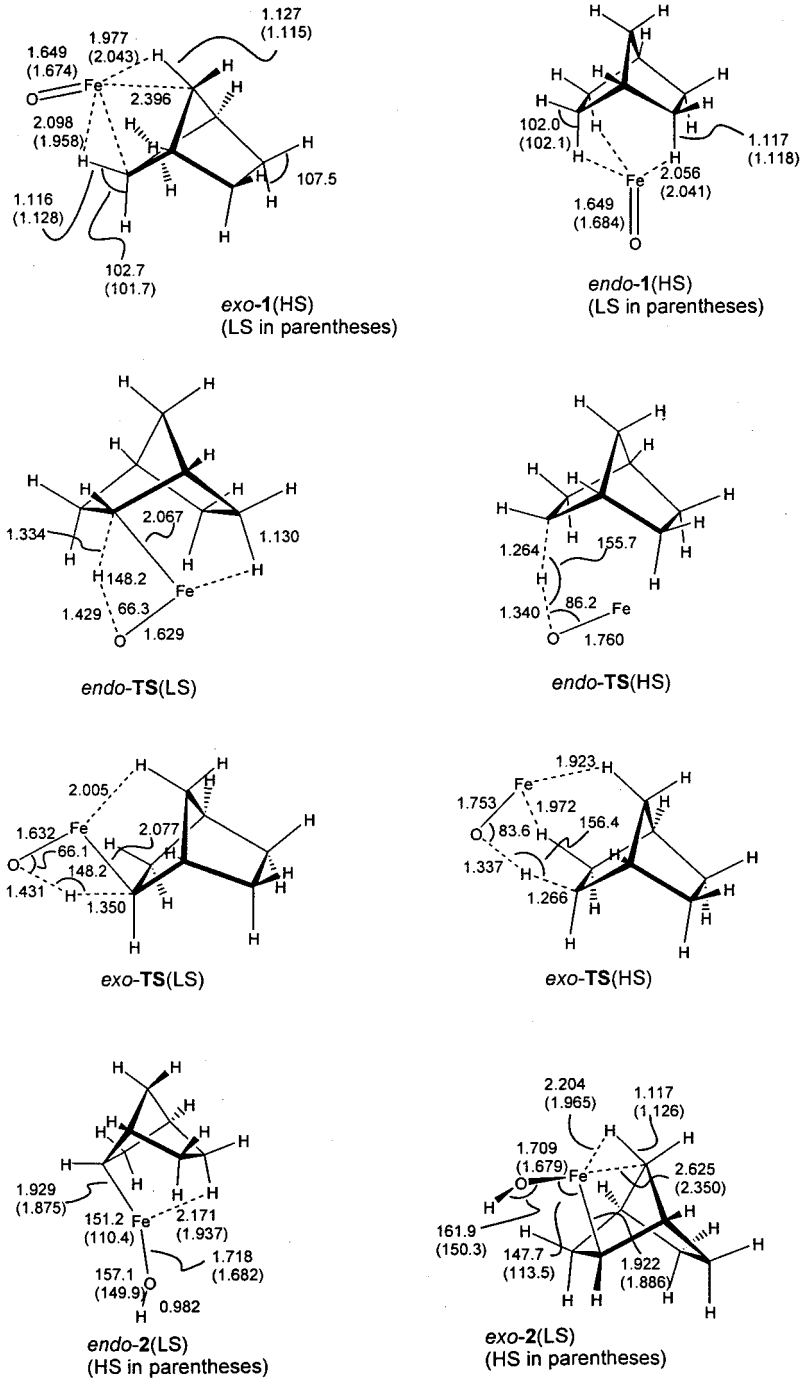

Fig. 1. *High-spin* (HS) *and low-spin* (LS) *structures for reactant clusters, transition structures, and insertion products for C–H bond activations computed at the B3LYP/6-31G** level of theory.* Key bond lengths, non-bonded contacts [Å], and bond angles [degree] are indicated.

distributed randomly among the normal modes. Furthermore, we assume that the *endo* and *exo* clusters can interconvert rapidly, *i.e.*, the (unknown) barrier for *endo*/*exo* equilibration, as well as the barriers associated with the rate-determining C–H bond activations, are anticipated to be small compared to the binding energy.

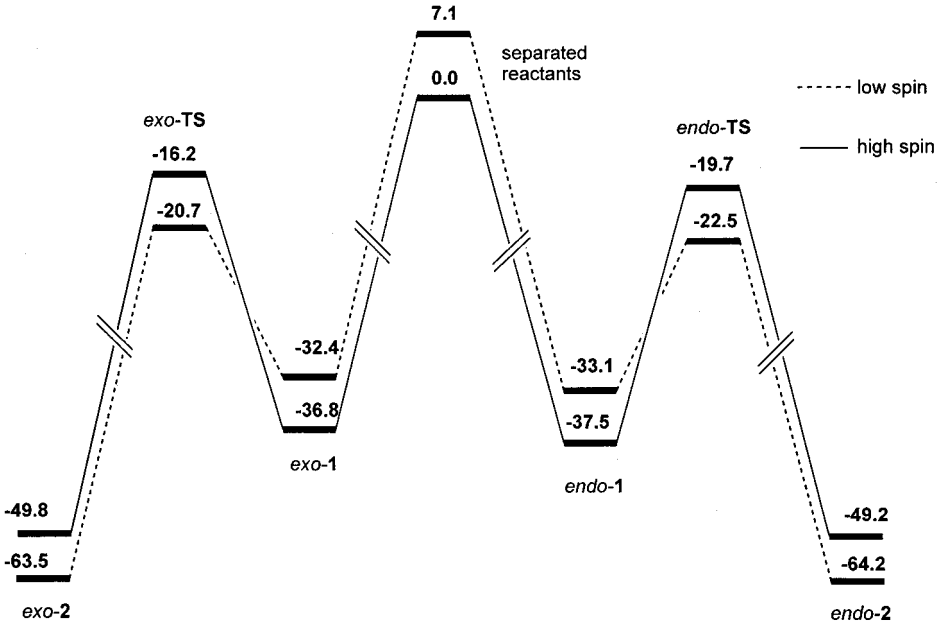

Fig. 2. *High-spin* (HS, S = 5/2) *and low-spin* (LS, S = 3/2) *potential-energy surfaces for* endo *and* exo *C–H bond activation of norbornane by FeO*$^+$. Energies are calculated at the B3LYP/6-31G** level of theory and are corrected for zero-point vibrational energy (ZVPE), except for the insertion products which are uncorrected. Note that this scheme does not include errors associated with the estimated BSSEs (see text).

For 3d metals, DFT is biased toward the $3d^n$ configuration compared to the $3d^{n-1}\,4s^1$ configuration [4g][27]. This causes the quartet spin states to be too stable relative to the sextet states, since the sextets have larger occupations of the 4s orbital. Another systematic error is spin symmetry of the quartet states of the free reactants and reactant clusters. These have $\langle S^2\rangle$ values of 4.4 compared to the expected value of 3.75 for a pure S = 3/2 state. Spin-symmetry deviation is not as serious for the low-spin TSs, which have $\langle S^2\rangle = 3.9$, and all structures with S = 5/2 have values close to the expected $\langle S^2\rangle = 8.75$. Thus, as with free FeO^+, the energies for the low-spin reactant clusters in *Fig. 2* should be adjusted upward by a few kcal · mol^{-1}.

Transition Structures. Previous DFT computational studies for H_2/FeO^+ and CH_4/FeO^+ showed that the TSs in the H–H and C–H bond activations are higher in energy than the separated reactants [4c][4f][4g][5c]. In contrast, the norbornane/FeO^+ reaction has TSs that are far below the entrance channel. From *Fig. 2*, the transition structure is at least 16 kcal · mol^{-1} below the reactants after including the zero-point vibrational energy (ZPVE). Inclusion of BSSE correction (assumed to be similar for the TS and the reactant cluster) still leaves the TSs at least 9 kcal · mol^{-1} below the

entrance channel. Location of the TSs for norbornane/FeO^+ well below the entrance channel accounts for the unit-reaction efficiency observed experimentally [14]. Thus, the reactant cluster is formed more or less irreversibly with respect to the separated reactants and then branches between *exo* and *endo* C–H bond activations. The low-spin TSs are more stable by 2.8 kcal · mol^{-1} (*endo*) and 4.5 kcal · mol^{-1} (*exo*) than the high-spin TSs. As mentioned above, the low-spin states are predicted to be too stable by DFT, and the separation between high- and low-spin TSs could be somewhat smaller.

As seen from *Fig. 1*, the high-spin TSs have the characteristics [5c,d] of a three-center atom-transfer mechanism (*b* in *Scheme 2*), while the low-spin TSs have characteristics [4g][5d] of a concerted four-center insertion mechanism (*a* in *Scheme 2*). In the HS structures, the C–H bonds to be cleaved have lengths of 1.26 Å, whereas the O–H bond lengths amount to 1.34 Å, and the Fe–C distances are almost unchanged compared to those in the reactant complexes. The O–H–C units are non-linear in either the HS or LS transition structures, but their angles are narrower in the LS structures by *ca.* 7°. An intrinsic reaction coordinate (IRC) following [18] for *exo*-**TS** (HS) gave support for the three-center mechanism; following the IRC led to shortening of the O–H bond with negligible change in the Fe–C distance. Other transition-metal oxidants, such as CrO_2Cl_2 and MnO_4^-, are also thought to react by three-center mechanisms, leading to radical pairs which then collapse to the products [24]. In our case, the radical pair does not seem to reside in a minimum. Optimization of structures obtained from the IRC calculations led to the *exo*-**2** (HS) product and not to a norbornyl/$FeOH^+$ diradical, in accord with previous results for the rebound mechanism in the FeO^+/H_2 system [4g].

The C–H and O–H bond lengths in the low-spin (LS) transition structures are 1.35 and 1.43 Å, respectively, and the Fe–C bond length is 2.07 Å (*Fig. 1*). Thus, the Fe–C bonds are almost fully formed, and the low-spin TSs lead to Fe–C-bonded products *exo*-**2** (LS) and *endo*-**2** (LS). These characteristics of the low-spin TS are similar to the computed TSs for the H_2/FeO^+ and CH_4/FeO^+ reactions in the four-center mechanism [4][5]. Compared to these substrates, a notable difference concerns the separation of the low- and high-spin TSs with norbornane. Thus, while the low-spin routes are clearly preferred for H_2 and CH_4, the energy differences of the low- and high-spin TSs amount to only a few kcal · mol^{-1} with norbornane. Conceptually, this can be rationalized by the sterically more congested situation of the Fe-atom with norbornane as a substrate in that close contact to both centers of the C–H bond to be activated results in enhanced, and also repulsive interaction with the backbone which is absent for H_2 and CH_4 as substrates. Further, note the embedding of the iron in the *endo*-TSs into the convex shape of the norbornane skeleton.

Products. From the transition structures, the reactions proceed downhill in energy to form the insertion products (*exo*-**2** and *endo*-**2**). As a consequence of the significant exothermicity of O–H bond formation, the insertion products are rovibrationally excited and rapidly undergo consecutive reactions. These secondary products can form by Fe–C bond homolysis or by rearrangement to the norborneol/Fe^+ complex, but the most likely route is *syn*-α-elimination to form a norbornene/$Fe(H_2O)^+$ cluster [14]. The latter species can subsequently lose the H_2O ligand and then yield the predominating $FeC_5H_6^+$ product ion concomitantly with neutral ethene *via* a retro-*Diels-Alder* reaction. Thus, we regard the insertion structure **2** as the key intermediate *en route* to

product formation. The high-spin structures *exo*-**2** (HS) and *endo*-**2** (HS) are 15 kcal·mol^{-1} (*endo*) and 14 kcal·mol^{-1} (*exo*) higher in energy than the low-spin structures (*Fig. 2*). As shown in *Fig. 1*, the B3LYP/6-31G** low-spin geometries have shorter Fe–C and Fe–O bounds, and narrower O–Fe–C angles than the high-spin structures, which is consistent with the conceptual descriptions of the insertion intermediates in the more simple H_2/FeO^+ and CH_4/FeO^+ systems [4][5].

exo/endo *Branching Ratios and Deuterium Isotope Effects.* Rate constants for the *endo* and *exo* C–H bond activations were computed with *RRKM* theory [28][3]). This uses the microcanonical ensembles, which apply to isolated molecules characterized by their internal energies *E*. This theory provides an appropriate model for the ICR experiments on the FeO^+/norbornane system performed under strictly bimolecular collison conditions. Our kinetic scheme assumes that the lifetime of the reactant cluster is long enough that the internal energy is statistically distributed among its normal vibrational modes. This is reasonable given that the ion/molecule clusters should have lifetimes on the order of microseconds in ICR experiments [14], which corresponds to the period for *ca.* 10^7 vibrations.

The *absolute* rate constants (*Table*) computed with the *RRKM* approach are subject to various errors caused by neglecting vibrational anharmonicity and rotational contributions to the sum and density of states. Neither of these systematic errors is serious in the present case, however, because we are concerned with only *relative* rates for branching of the cluster between two alternative pathways. In fact, the uncertainty in our computed branching ratios is primarily determined by errors of the potential-energy surfaces, *i.e.*, the computed binding energies of the clusters, the barrier heights, and the HS/LS energy gaps.

The ratio of *RRKM* rates k_a/k_b for branching from a common ground state by two pathways (a) and (b) are given by N_a^*/N_b^*, where N_a^* and N_b^* are the numbers of states for two transition structures a and b with activation barriers E_a^* and E_b^* [28]. For example, the kinetic isotope effect (k_H/k_D) for C–H(D) bond activation of [2-D_1]norbornane by FeO^+ is given by N_H^*/N_D^*, and, similarly, the *endo*/*exo* branching ratio is given by N_{endo}^*/N_{exo}^*. The number densities depend on the harmonic frequencies and moments of inertia of the TSs, and on the energy terms ($E - E^*$), which are the differences between the respective TSs and the entrance channel. Plots of *endo*/*exo* branching ratio and KIEs *vs.*

---

[3]) *endo*/*exo* Branching ratios and kinetic isotope effects were computed with *Rice-Ramsperger-Kassel-Marcus* (*RRKM*) theory [28]. This uses the harmonic vibrational frequencies for the ground and transition structure to compute the microcanonical rate constant $k(E)$ as a function of internal energy. The frequencies were used for evaluation of the sum of states and density of states needed in the *RRKM* equation by direct count with the algorithm of *Beyer* and *Swinehart* [28d]. The *RRKM* unimolecular rate constant was computed according to *Eqn. 1.*

$$k(E) = \sigma \cdot N^*(E - E^*)/(h \cdot \rho(E)) \quad (1)$$

Here, σ is the symmetry number ($\sigma = 4$ in our case, because norbornane has four equivalent *exo* C–H bounds and four equivalent *endo* C–H bonds), h is *Planck*'s constant, $N^*(E - E^*)$ is the sum of states for the transition structure having internal vibrational energy ($E - E^*$), E^* is the barrier height, and $\rho(E)$ is the density of states for the ground structure having internal vibrational energy E. Rotational contributions to the sum and density of states were ignored; it was assumed that the internal energy in the reactant clusters and the transition structures are distributed entirely in the vibrational modes. Branching ratios and KIEs were computed from the microcanonical rate constants as described below.

Table. *Summary of* RRKM *Results for C–H Bond Activation of Norbornane by FeO^+ at Different Internal Energies Relative to the Most Stable Reactant Complex* endo-**1** *(HS)*

Absolute rate constants [a])			
Energy [kcal·mol^{-1}]	$k_{HS}(E)$ [s^{-1}]	$k_{LS}(E)$ [s^{-1}]	k_{LS}/k_{HS}
25	$2.4\cdot10^5$	$6.4\cdot10^6$	27
30	$2.1\cdot10^6$	$2.9\cdot10^7$	14
35	$9.9\cdot10^6$	$9.0\cdot10^7$	9

Branching ratios k_{endo}/k_{exo} [b])			
Energy [kcal·mol^{-1}]	Isotope	High-spin	Low-spin
25	Protio	67	5.4
30		19	3.7
35		10	3.0
30	[*exo*-2-D_1]	62	9.8
30	[*endo*-2-D_1]	6.6	1.6

Kinetic isotope effects [c, d])				
Energy [kcal·mol^{-1}]	High-spin		Low-spin	
	exo	*endo*	*exo*	*endo*
25	6.1	3.8	3.3	2.8
30	3.3	2.9	2.9	2.3
35	2.6	2.5	2.3	2.1

[a]) Absolute rate constants are combined rates for *exo* and *endo*, *i.e.*, $k(E)=k(E)_{exo}+k(E)_{endo}$. [b]) Experimental value: $k_{endo}/k_{exo}=10.3$ [14a]. [c]) Intramolecular KIEs associated with C–H(D) bond activation of [*exo*-2-D_1]- and [*endo*-2-D_1]norbornane, respectively. [d]) Experimental values: $KIE_{endo}=2.4$ and $KIE_{exo}=7.7$ [14a].

internal energy are shown in *Figs. 3* and *4*. The energy scale for these plots is 25–35 kcal·mol^{-1}, which was chosen based on our 30 kcal·mol^{-1} estimate for the binding energy of the cluster after correction for BSSE. Error in the computed barrier heights (*i.e.*, energy of the TSs relative to the clusters) causes the curves in *Fig. 3* to shift to the left if the barriers are too small, and to the right if they are too large.

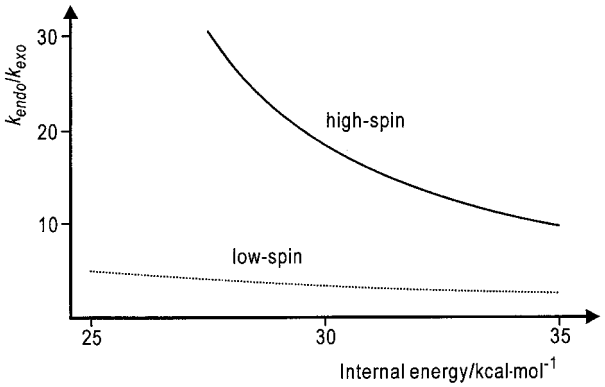

Fig. 3. endo/exo *Branching ratios for C–H bond activations on the high-* (solid line) *and low-spin* (dotted line) *surfaces, computed from the B3LYP/6-31G** harmonic frequencies according to* RRKM *theory.* The rates are plotted as a function of internal energy of the reactant clusters relative to *endo*-**1** (HS).

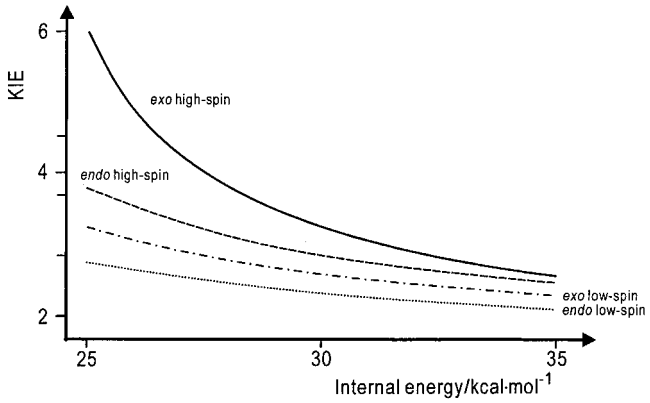

Fig. 4. *Kinetic isotope effects* (KIE = k_H/k_D) *associated with* endo *and* exo *C–H bond activations of norbornane computed from B3LYP/6-31G** harmonic frequencies according to* RRKM *theory.* The rates are plotted as a function of internal energy of the reactant clusters relative to *endo*-**1** (HS); *solid line:* KIE_{exo} (HS), *dashed line:* KIE_{endo} (HS), *dotted-dashed line:* KIE_{exo} (LS), *dotted line:* KIE_{endo} (LS).

The computed k_H/k_D and *endo*/*exo* ratios (*Figs. 3* and *4*) are determined mainly by differences in barrier heights for the competing pathways; the more favorable pathways have lower barriers. The computed barrier heights for the *exo* transition structures are larger than for the corresponding *endo* transition structures. Thus, the relative energy for *exo*-**TS** (HS) is higher than that for *endo*-**TS** (HS) by 3.5 kcal · mol^{-1}, and the energy for *exo*-**TS** (LS) is higher than that for *endo*-**TS** (LS) by 1.8 kcal · mol^{-1}. Consequently, a ratio $k_{endo}/k_{exo} \gg 1$ results for both high- and low-spin paths.

At $E = 30$ kcal · mol^{-1}, the computed *endo*/*exo* branching ratios (*Table*) are 19.0 (high spin) and 3.7 (low spin), compared with the experimental k_{endo}/k_{exo} ratio of 10.3 [14a]. The downward slopes of the curves in *Fig. 3* show that the selectivities of the *endo* paths decrease as the internal energy increases. This is the usual trade-off between internal energy, *viz.* effective temperature, and selectivity. The preference for *endo* C–H bond activation agrees with observed *endo* preference for MnO_4^- oxidation of norbornane in solution [29], but not with the preference for *exo* C–H bond activation in hydroxylations of norbornane and camphor by P-450 and model complexes [13].

The branching of C–H *vs.* C–D bonds is controlled by the *ca.* 1.0 kcal · mol^{-1} difference in barrier heights between two related transition structures differing only in isotopic substitution. The difference in barriers is primarily associated with the larger zero-point energy for migration of the heavier isotope. The primary isotope effects cause the *endo*/*exo* ratios to shift in favor of C–H bond rather than C–D bond activation. For example, at $E = 30$ kcal · mol^{-1} on the high-spin surface, the *endo*/*exo* ratio of 19 for unlabeled norbornane increases to 62 for [*exo*-2-D_1]norbornane, but amounts to only 6.6 for the [*endo*-2-D_1]-isotopomer (*Table*). Thus, stereoselective deuteration at C(2) in norbornane alters the *endo*/*exo* ratios by almost one order of magnitude; such effects are known as isotopically sensitive branching or metabolic switching, and have been observed earlier in hydroxylation of labeled ethylbenzene by cytochrome P-450 [30].

The observed $KIE_{exo} = 7.7$ [14a] is in good agreement with the computed KIE_{exo} of the high-spin pathway (*Fig. 4*), while the observed $KIE_{endo} = 2.4$ agrees best with the data for the low-spin route. If the analysis of the experimental data is accurate[4]), our results suggest that the *exo* pathway proceeds mainly *via* the high-spin TS and the *endo* pathway mainly *via* the low-spin TS. At any energy, the curves in *Fig. 4* show that the KIEs can give a useful distinction between the low- and high-spin mechanisms. In particular, the large KIE_{exo} implies that the high-spin surface, *i.e.*, SSR, contributes to the observed reactivity. This, in turn, means that spin crossover is a bottleneck in the reactions, but with different selectivities for the *endo* and the *exo* pathways.

Spin Crossover. The excess energy of the clusters enables both SSR (none or complete crossing) as well as TSR (crossing along the reaction coordinate) in the norbornane/FeO^+ system. For a conceptual analysis, let us first consider the two extremes. *i*) If the rate constant associated with intersystem crossing (k_x) is small ($k_x \ll k_{HS}$), the entire reaction takes place on the sextet surface, *i.e.*, exclusive SSR. *ii*) A second possibility is that the intersystem crossing is very fast ($k_x \gg k_{HS}$), so the low- and high-spin reactant clusters equilibrate [31]. As the low-spin barriers are lower than the high-spin TSs, this results in an exclusive passage *via* the LS route, which can again be described in terms of SSR, because spin inversion does not contribute to the rate-determining steps. If, however, k_x and k_{HS} are similar and the crossing takes place along the reaction coordinate, effective competition between SSR and TSR is expected. This means the minimum-energy crossing point (MECP) is found in the vicinity of the TS, and not near the reactants or products. This is likely in our case, because the vertical energy difference between the high- and low-spin surfaces at the high-spin TS is quite small; our computations at the B3LYP/6-31G** level indicate a difference of only $0.9\ kcal \cdot mol^{-1}$ ($E_{HS} - E_{LS}$) in both the *endo*- and *exo*-TSs. Accordingly, along the reaction coordinate from the reactant clusters to the respective TSs, the probability of spin inversion from the high- to the low-spin surfaces increases, thereby allowing for a complex interplay between SSR and TSR pathways. For the norbornane/FeO^+ system, it may not be possible to choose which scenario is most appropriate, but we can favor the third scenario based on the experimental KIE and k_{endo}/k_{exo} values, because the two other extreme scenarios do not fit the experimental data well. The best correspondence to experiment would arise if the *exo* C–H bond activation proceeded mainly *via* SSR (large KIE), while the *endo* C–H bond activation involves a more equal mixture of SSR and TSR. Such a picture would imply that the spin-inversion probability is smaller for the *exo* C–H bond activation. Indeed, the somewhat smaller adiabatic LS/HS energy difference of the *endo* path (*Fig. 2*) is consistent with this suggestion, because a smaller gap gives rise to better *Franck-Condon* factors and hence somewhat more efficient spin-orbit coupling in the *endo* route [32].

---

[4]) In the evaluation of the *endo*/*exo* ratio and the associated KIEs, isotopic scrambling has been neglected, even though the amount of H/D equilibration shows a significant dependence on the stereochemistry of the labeling, *i.e.*, about twice as much scrambling for the *endo*-labeled compound [14a]. Further, note that the branching ratio is the most sensitive parameter in the unconvolution of the experimental data, and the *RRKM* results also predict a more pronounced energy dependence compared to the KIEs.

Conclusions. – In the mechanism for C–H bond activation of norbornane by FeO^+, the reactants form clusters with binding energies of *ca.* 30 kcal · mol^{-1}. In these clusters, the FeO^+ unit binds at the *exo* or *endo* norbornane faces, allowing the electron-deficient iron to maximize agostic contacts with the polarizable norbornane surface. The C–H bond-activation steps take place from the clusters *via* low- ($S = 3/2$) and high-spin ($S = 5/2$) transition structures, leading to the corresponding insertion intermediates. Due to the driving force provided by O–H bond formation, the insertion intermediates are formed in rovibrationally excited states and react rapidly to form the secondary products described in previous ICR experiments [14]. Interesting differences are found in the high- and low-spin transition structures. Three high-spin TSs resemble three-center H-atom transfers [24], while the low-spin TSs resemble concerted four-center insertions of FeO^+ into the C–H bond [4g][15a]. The vertical energy difference between the high- and low-spin TS is quite small, so our model suggests spin crossing can take place near the high-spin TS, leading to SSR/TSR competition. The *endo*/*exo* branching and kinetic isotope effects determined in the experiments are conveniently modeled by *RRKM* theory. The best match between experimental and computed data involves an interesting scenario in which *exo* C–H bond activation occurs mainly *via* the high-spin path, while *endo* C–H bond activation occurs *via* a mixture of high- and low-spin pathways.

This research is supported by the *Volkswagen-Stiftung*, the *Deutsche Forschungsgemeinschaft*, the *Fonds der Chemischen Industrie*, and the *German-Israeli Foundation* (*G.I.F.*). *N. H.* is partially supported by a fellowship from the *U.S.-Israeli Fulbright Foundation. S. S.* acknowledges the *Alexander von Humboldt-Stiftung* for a *Humboldt Senior* research award. Dr. *Jeremy Harvey*, University of Bristol, is thanked for providing a version of his *RRKM* program. We are grateful to the *Konrad Zuse Zentrum*, Berlin, for generous allocation of computing time.

REFERENCES

[1] M. R. A. Pavlov, M. R. A. Blomberg, P. E. M. Siegbahn, R. Wesendrup, C. Heinemann, H. Schwarz, *J. Phys. Chem. A* **1997**, *101*, 1567; b) R. H. Hertwig, K. Seemeyer, H. Schwarz, W. Koch, *Chem. Eur. J.* **1997**, *3*, 1315; c) P. A. M. van Koppen, M. T. Bowers, C. L. Haynes, P. B. Armentrout, *J. Am. Chem. Soc.* **1998**, *120*, 5704.

[2] a) M. C. Holthausen, C. Heinemann, H. H. Cornehl, W. Koch, H. Schwarz, *J. Chem. Phys.* **1995**, *102*, 4931; b) M. C. Holthausen, W. Koch, *J. Am. Chem. Soc.* **1996**, *118*, 9932; c) A. Fiedler, D. Schröder, W. Zummack, H. Schwarz, *Inorg. Chim. Acta* **1997**, *259*, 227.

[3] a) W. J. Hehre, L. Radom, P. v. R. Schleyer, J. A. Pople, 'Ab Initio Molecular Orbital Theory', Wiley Interscience, New York, 1986; b) R. G. Parr, W. Yang, *Annu. Rev. Phys. Chem.* **1995**, *46*, 701; c) T. Ziegler, in ACS Symposium series 593, 'Chemical Applications of Density Functional Theory', Ed. B. Laird, American Chemical Society, Washington D.C., 1996; d) T. Ziegler, in ACS Symposium series 677, 'Computational Thermochemistry', Ed. K. K. Irikura, American Chemical Society, Orlando, 1998.

[4] a) D. Schröder, A. Fiedler, M. F. Ryan, H. Schwarz, *J. Phys. Chem.* **1994**, *98*, 68; b) D. E. Clemmer, Y.-M. Chen, F. A. Khan, P. B. Armentrout, *ibid.*, **1994**, *98*, 6522; c) A. Fiedler, D. Schröder, S. Shaik, H. Schwarz, *J. Am. Chem. Soc.* **1994**, *116*, 7815; d) V. Baranov, G. Javahery, A. C. Hopkinson, D. K. Bohme, *ibid.* **1995**, *117*, 12801; e) D. Schröder, H. Schwarz, D. E. Clemmer, Y. Chen, P. B. Armentrout, V. I. Baranov, D. K. Bohme, *Int. J. Mass Spectrom. Ion Processes* **1997**, *161*, 175; f) D. Danovich, S. Shaik, *J. Am. Chem. Soc.* **1997**, *119*, 1773; g) M. Filatov, S. Shaik, *J. Phys. Chem. A* **1998**, *102*, 3835.

[5] a) D. Schröder, H. Schwarz, *Angew. Chem.* **1990**, *102*, 1468; *ibid. Int. Ed.* **1990**, *29*, 1433; b) D. Schröder, A. Fiedler, J. Hrušák, H. Schwarz, *J. Am. Chem. Soc.* **1992**, *114*, 1215; c) K. Yoshizawa, Y. Shiota, T. Yamabe, *ibid.* **1998**, *120*, 564; d) K. Yoshizawa, Y. Shiota, T. Yamabe, *Organometallics* **1998**, *17*, 2825; e) K. Yoshizawa, Y. Shiota, T. Yamabe, *J. Chem. Phys.* **1999**, *111*, 538.

[6] a) D. Schröder, H. Schwarz, *Helv. Chim. Acta* **1992**, *75*, 1281; b) H. Becker, D. Schröder, W. Zummack, H. Schwarz, *J. Am. Chem. Soc.* **1994**, *116*, 1096; c) K. Yoshizawa, Y. Shiota, T. Yamabe, *ibid.* **1999**, *121*, 147.
[7] a) D. Schröder, H. Schwarz, *Angew. Chem.* **1995**, *107*, 2023, *ibid. Int. Ed.* **1995**, *34*, 1973; b) D. Schröder, H. Schwarz, S. Shaik, in 'Structure and Bonding', Ed. B. Meunier, Springer Verlag, Berlin, in preparation.
[8] a) 'Cytochrome P-450: Structure, Mechanisms and Biochemistry', Ed. P. R. Ortiz de Montellano, 2nd edn., Plenum Press, New York, 1995; b) M. Sono, M. P. Roach, E. D. Coulter, M. H. Dawson, *Chem. Rev.* **1996**, *96*, 2845; c) W.-D. Woggon, *Top. Curr. Chem.* **1997**, *184*, 46.
[9] P-450 reviews: a) J. T. Groves, *J. Chem. Ed.* **1985**, *62*, 928; b) S. K. Chapman, S. Daff, A. W. Munro, in 'Structure and Bonding', Springer Verlag: Berlin, **1997**, *88*, p. 40; c) T. G. Traylor, P. S. Traylor, in 'Active Oxygen in Biochemistry', Eds. J. S. Valentine, C. S. Foote, A. Greenberg, J. F. Liebman, Blackie Academic and Professional, New York, **1995**, Chapt. 3.
[10] a) K. A. Lee, W. Nam, *J. Am. Chem. Soc.* **1997**, *119*, 1916; b) K. Kamaraj, D. Bandyopadhyay, *J. Am. Chem. Soc.* **1997**, *119*, 8099; c) A. D. N. Vaz, D. F. McGinnity, M. J. Coon, *Proc. Natl. Acad. Sci. U.S.A.* **1998**, *95*, 3555.
[11] a) J. Antony, M. Grodzicki, A. X. Trautwein, *J. Phys. Chem. A* **1997**, *101*, 2692; b) M. Filatov, N. Harris, S. Shaik, *J. Chem. Soc., Perkin Trans. 2* **1999**, 399.
[12] a) P. E. M. Siegbahn, R. H. Crabtree, *J. Am. Chem. Soc.* **1997**, *119*, 3103; b) K. Yoshizawa, T. Ohta, T. Yamabe, *Bull. Chem. Soc. Jpn.* **1998**, *71*, 1899; c) A. L. Feig, S. J. Lippard, *Chem. Rev.* **1994**, *94*, 759.
[13] a) J. T. Groves, G. A. McClusky, R. E. White, M. Coon, *J. Biochem. Biophys. Res. Commun.* **1978**, *81*, 154; b) M. H. Gelb, D. C. Heimbrook, P. Malkonen, S. G. Sligar, *Biochemistry* **1982**, *21*, 370; c) T. G. Traylor, K. W. Hill, W.-P. Fann, S. Tsuchiya, B. E. Dunlap, *J. Am. Chem. Soc.* **1992**, *114*, 1308; d) A. Sorokin, A. Robert, B. Meunier, *ibid.* **1993**, *115*, 7293; e) D. Dolphin, T. G. Traylor, L. Y. Xie, *Acc. Chem. Res.* **1997**, *30*, 251.
[14] a) J. Schwarz, H. Schwarz, *Helv. Chim. Acta* **1995**, *78*, 1013; b) J. Schwarz, R. Wesendrup, D. Schröder, H. Schwarz, *Chem. Ber.* **1996**, *129*, 1463; c) J. Schwarz, Dissertation, TU Berlin, D83, Shaker Verlag, Aachen, 1996.
[15] a) S. Shaik, D. Danovich, A. Fiedler, D. Schröder, H. Schwarz, *Helv. Chim. Acta* **1995**, *78*, 1393 – 1407; b) D. A. Plattner, *Angew. Chem.* **1999**, *111*, 86, *ibid. Int. Ed.* **1999**, *38*, 82.
[16] a) S. Shaik, M. Filatov, D. Schröder, H. Schwarz, *Chem. Eur. J.* **1998**, *4*, 193; b) P. H. Toy, M. Newcomb, P. F. Hollenberg, *J. Am. Chem. Soc.* **1998**, *120*, 7719; c) N. Jin, J. T. Groves, *J. Am. Chem. Soc.* **1999**, *121*, 2923.
[17] a) M. Newcomb, M.-H. Le Tadic, D. A. Putt, P. F. Hollenberg, *J. Am. Chem. Soc.* **1995**, *117*, 3312; b) M. Newcomb, M.-H. Le Tadic-Biadatti, D. L. Chestrey, E. S. Roberts, P. F. Hollenberg, *J. Am. Chem. Soc.* **1995**, *117*, 12085.
[18] Gaussian 94, Revision E.2, Gaussian Inc., Pittsburgh PA, 1995.
[19] a) C. Lee, W. Yang, R. G. Parr, *Phys. Rev.* **1988**, *B37*, 785; b) A. D. Becke, *J. Chem. Phys.* **1993**, *98*, 5648; *ibid.* **1992**, *96*, 2155; *ibid.* **1992**, *97*, 9173; c) P. J. Stephens, F. J. Devlin, C. F. Chabalowski, M. J. Frisch, *J. Phys. Chem.* **1994**, *98*, 11623.
[20] M. J. Frisch, A. Frisch, J. B. Foresman, 'Gaussian 94 User's Reference', Gaussian Inc., Pittsburgh, PA, 1994, and references therein.
[21] a) A. Schafer, H. Horn, R. Ahlrichs, *J. Chem. Phys.* **1992**, *97*, 2571; b) 'Extensible Computational Chemistry Environment Basis Set Database', Version 1.0, as developed and distributed by the Molecular Science Computing Facility, Pacific Northwest Laboratory, P.O. Box 999, Richland, Washington 99352, USA. http://www.emsl.pnl.gov:2080/forms/basisform.html.
[22] A. Fiedler, J. Hrušák, W. Koch, H. Schwarz, *Chem. Phys. Lett.* **1993**, *211*, 242.
[23] J. Husband, F. Aguirre, P. Ferguson, R. Metz, *J. Chem. Phys.* **1999**, *111*, 1433.
[24] a) A. K. Rappe, W. A. Goddard, *J. Am. Chem. Soc.* **1982**, *104*, 3287; b) D. G. Lee, T. Chen, *ibid.* **1993**, *115*, 11231; c) G. K. Cook, J. M. Mayer, *ibid.* **1995**, *117*, 7139; d) T. Ziegler, J. Li, *Organometallics* **1995**, *14*, 214; e) K. A. Gardner, L. L. Kuehnert, J. M. Mayer, *Inorg. Chem.* **1997**, *36*, 2069; f) L. Deng, T. Ziegler, *Organometallics* **1997**, *16*, 716.
[25] J. P. Collman, A. S. Chien, T. A. Eberspacher, J. I. Brauman, *J. Am. Chem. Soc.* **1998**, *120*, 425.
[26] J. M. L. Martin, J. P. Francois, R. Gijbels, *Theor. Chim. Acta* **1989**, *76*, 195, and ref. cit. therein.
[27] a) R. D. Bach, D. S. Shobe, H. B. Schlegel, C. J. Nagel, *J. Phys. Chem.* **1996**, *100*, 8770; b) C. W. Bauschlicher, Jr., *Chem. Phys.* **1996**, *211*, 163; c) M. N. Glukhovtsev, R. D. Bach, C. J. Nagel, *J. Phys. Chem. A* **1997**, *101*, 316.

[28] a) P. J. Robinson, K. A. Holbrook, 'Unimolecular Reactions', Wiley Interscience, London, 1972; b) D. A. McQuarrie, 'Statistical Thermodynamics', Harper and Row, New York, 1973; c) M. J. Pilling, P. W. Seakins, 'Reaction Kinetics', Oxford Press, Oxford, 1995; d) T. Baer, W. L. Hase, 'Unimolecular Reaction Dynamics', Oxford Press, Oxford, 1996.
[29] H. Kwart, *J. Am. Chem. Soc.* **1960**, *82*, 2348.
[30] R. E. White, J. P. Miller, L. V. Favreau, A. Bhattacharyya, *J. Am. Chem. Soc.* **1986**, *108*, 6024.
[31] a) E. V. Dose, M. A. Hoselton, N. Sutin, M. F. Tweedle, L. J. Wilson, *J. Am. Chem. Soc.* **1978**, *100*, 1141; b) D. Schröder, C. Heinemann, H. Schwarz, J. N. Harvey, S. Dua, S. J. Blanksby, J. H. Bowie, *Chem. Eur. J.* **1998**, *4*, 2550.
[32] H. Lefevre-Brion, R. W. Field, 'Perturbations in the Spectra of Diatomic Molecules', Academic Press, New York, 1986.

Received August 21, 1999